Monthly Notices of the ROYAL ASTRONOMICAL SOCIETY

Mon. Not. R. Astron. Soc. **415,** 1950–1960 (2011) doi:10.1111/j.1365-2966.2011.18840.x

A pilot study for the SCUBA-2 'All-Sky' Survey

Todd Mackenzie,[1*] Filiberto G. Braglia,[1] Andy G. Gibb,[1] Douglas Scott,[1]
Tim Jenness,[2] Stephen Serjeant,[3] Mark Thompson,[4] David Berry,[2]
Christopher M. Brunt,[5] Edward Chapin,[1] Antonio Chrysostomou,[2] Dave Clements,[6]
Kristen Coppin,[7,8] Frossie Economou,[2] A. Evans,[9] Per Friberg,[2] Jane Greaves,[10]
T. Hill,[11] Wayne Holland,[12,13] R. J. Ivison,[12,13] Johan H. Knapen,[14,15] Neal Jackson,[16]
Gilles Joncas,[17] Larry Morgan,[18] Angela Mortier,[6] Chris Pearson,[19,20,3]
Michele Pestalozzi,[21] Alexandra Pope,[22] John Richer,[23,24] J. S. Urquhart,[25]
Mattia Vaccari,[26] Bernd Weferling,[27] Glenn White[3,19] and Ming Zhu[28]

[1] *Department of Physics and Astronomy, University of British Columbia, 6224 Agricultural Road, Vancouver, BC V6T 1Z1, Canada*
[2] *Joint Astronomy Centre, 660 North A'ohoku Place, Hilo, HI 96720, USA*
[3] *Department of Physics and Astronomy, The Open University, Milton Keynes MK7 6BJ*
[4] *Centre for Astrophysics Research, Science and Technology Research Institute, University of Hertfordshire, College Lane, Hatfield AL10 9AB*
[5] *School of Physics, Stocker Road, Exeter EX4 4QL*
[6] *Imperial College London, South Kensington Campus, London SW7 2AZ*
[7] *Department of Physics, McGill University, 3600 rue University, Montréal, QC H3A 2T8, Canada*
[8] *Institute for Computational Cosmology, Durham University, South Road, Durham DH1 3LE*
[9] *Astrophysics Group, Keele University, Keele, Staffordshire ST5 5BG*
[10] *School of Physics and Astronomy, University of St Andrews, North Haugh, St Andrews KY16 9SS*
[11] *Laboratoire AIM, CEA/IRFU – CNRS/INSU – Université Paris Diderot, CEA-Saclay, 91191 Gif-sur-Yvette Cedex, France*
[12] *UK Astronomy Technology Centre, Royal Observatory, Blackford Hill, Edinburgh EH9 3HJ*
[13] *Institute for Astronomy, University of Edinburgh, Blackford Hill, Edinburgh EH9 3HJ*
[14] *Instituto de Astrofísica de Canarias, E-38200 La Laguna, Tenerife, Spain*
[15] *Departamento de Astrofísica, Universidad de La Laguna, E-38205 La Laguna, Tenerife, Spain*
[16] *Jodrell Bank Centre for Astrophysics, Alan Turing Building, School of Physics and Astronomy, University of Manchester, Oxford Road, Manchester M13 9PL*
[17] *Dépt. de physique, de génie physique et d'optique and Centre de recherche en astrophysique du Québec, Université Laval, Québec G1V 0A6, Canada*
[18] *Astrophysics Research Institute, Liverpool John Moores University, Twelve Quays House, Egerton Wharf, Birkenhead, Wirral CH41 1LD*
[19] *RAL Space, Rutherford Appleton Laboratory, Chilton, Didcot, Oxfordshire OX11 0QX*
[20] *Institute for Space Imaging Science, University of Lethbridge, Lethbridge, Alberta T1K 3M4, Canada*
[21] *IFSI/INAF, via del Fosso del Cavaliere 100, I–00173 Roma, Italy*
[22] *Department of Astronomy, University of Massachusetts, 710 North Pleasant Street, Amherst, MA 01003-9305, USA*
[23] *Astrophysics Group, Cavendish Laboratory, J. J. Thomson Avenue, Cambridge CB3 0HE*
[24] *Kavli Institute for Cosmology, c/o Institute of Astronomy, University of Cambridge, Madingley Road, Cambridge CB3 0HA*
[25] *Australia Telescope National Facility, CSIRO Astronomy and Space Science, Sydney, NSW 2052, Australia*
[26] *Department of Astronomy, University of Padova, Vicolo Osservatorio 3, I-35122 Padova, Italy*
[27] *University Bamberg, Markusplatz 3, 96045 Bamberg, Germany*
[28] *National Astronomical Observatories, Chinese Academy of Sciences, A20 Datun Road, Chaoyang District, Beijing, China*

Accepted 2011 April 3. Received 2011 March 14; in original form 2010 December 8

ABSTRACT

We have carried out a pilot study for the Submillimetre Common-User Bolometer Array 2 (SCUBA-2) 'All-Sky' Survey (SASSy), a wide and shallow mapping project at 850 μm, designed to find rare objects, both Galactic and extragalactic. Two distinct sets of exploratory observations were undertaken and used to test the SASSy approach and data-reduction pipeline. The first was a $0\overset{\circ}{.}5 \times 0\overset{\circ}{.}5$ map around the nearby galaxy NGC 2559. The galaxy was easily detected at 156 mJy, but no other convincing sources are present in the map. Comparison with

---

[*] E-mail: todd@phas.ubc.ca

other galaxies with similar wavelength coverage indicates that NGC 2559 has relatively warm dust. The second observations cover 1 deg^2 around the W5-E H II region. As well as diffuse structure in the map, a filtering approach was able to extract 27 compact sources with signal-to-noise ratio greater than 6. By matching with data at other wavelengths we can see that the SCUBA-2 data can be used to discriminate the colder cores. Together these observations show that the SASSy project will be able to meet its original goals of detecting new bright sources which will be ideal for follow-up observations with other facilities.

Key words: surveys – submillimetre: galaxies – submillimetre: stars.

1 INTRODUCTION

The millimetre and submillimetre (submm) parts of the electromagnetic spectrum directly probe the cold Universe. The submm window specifically allows us to study the youngest phases of star formation in our Galaxy and the dusty, most prodigiously star-forming galaxies at high redshift. Despite this strong motivation, the submm sky still remains poorly surveyed. The Submillimetre Common-User Bolometer Array 2 (SCUBA-2) 'All-Sky' Survey (SASSy)[1] is a James Clerk Maxwell Telescope (JCMT) Legacy Survey project designed to redress this balance and exploit the rapid mapping capability of SCUBA-2 to ultimately map a large portion of the sky visible from the JCMT to an angular resolution of 14 arcsec at 850 μm. The target point source rms level is 30 mJy.

The benefits of such a wide-field survey are many, ranging from a complete census of infrared (IR) dark clouds to the potential discovery of some of the most luminous high-redshift galaxies in the Universe (Thompson et al. 2007). The approved phase of SASSy consists of two distinct parts: a strip covering the Galactic plane which is visible from Hawaii and a 'pole-to-pole' strip perpendicular to this and designed to pass through the Galactic and ecliptic north poles. These observations will be carried out in 'Grade 4' weather conditions ($0.12 < \tau_{225} < 0.2$, where τ_{225} is the sky opacity at 225 GHz, as measured by the Caltech Submillimeter Observatory radiometer), i.e. essentially when the atmosphere is too opaque to enable useful observations of fainter objects with SCUBA-2. The 450-μm data are therefore expected to be of marginal value, and the survey is entirely designed to make large maps at 850 μm, with a target sensitivity of 30 mJy, achieved using a fast scanning speed.

SASSy will be able to build on the success of *IRAS* at one decade shorter wavelengths. It is also complementary to several more recent wide surveys, namely *WISE* and *AKARI*, at near- and mid-IR wavelengths, and surveys with the *Herschel* and *Planck* satellites in the submm. Early results from *Herschel* have already demonstrated that bright lensed galaxies can be selected at submm wavelengths (Negrello et al. 2010), and also that potentially protostellar cores can also be found using *Herschel* (Ward-Thompson et al. 2010). The *Planck* Early Release Compact Source Catalogue will contain an all-sky list of sources which includes the 850-μm channel. However, the resolution of SASSy will be 20 times better. Hence, it is clear that if SCUBA-2 is able to map rapidly enough while maintaining its nominal beamsize and achieving the required sensitivity then SASSy will be able to meet its science goals. As we show below, these preliminary SCUBA-2 data lend confidence that these requirements can be met and that SASSy will discover many new and interesting sources.

In the next section we describe the two sets of observations which were made as a pilot study for SASSy, one Galactic field and one extragalactic field. In Section 3 we describe how we reduced the data and extracted sources. We then discuss the properties of the sources that we found and end with some conclusions about SASSy in general.

2 OBSERVATIONS

SCUBA-2 (Holland et al. 2003, 2006) is the successor to the SCUBA (Holland et al. 1999), which operated successfully on the JCMT from 1997 to 2005. SCUBA-2 has been designed to be hundreds of time faster than SCUBA for mapping the sky in the same two primary bands, 450 and 850 μm. The observatory offered a period of 'Shared Risks Observing' programme (hereafter S2SRO), in which relatively short programmes were carried out with a partially commissioned version of the instrument, having one (of the four) subarray available at each of the two bands. Unless stated otherwise, all maps and detections in this paper are at 850 μm, since this is the primary wavelength of interest for SASSy.

As part of S2SRO there were two separate sets of observations carried out for SASSy, which we now describe. The SCUBA-2 array of 32 × 40 transition-edge sensitive bolometers has a footprint of about 3 arcmin^2 on the sky (it will double in linear size when the focal plane is fully populated with subarrays), and takes data at a sampling rate of approximately 200 Hz while scanning across the selected region. The available 850-μm array typically only had 50 per cent of the detectors working (although the number used in the data reduction is selected dynamically and hence varies with time). Calibration was performed using an internal flat-field source, as well as absolute measurements using known calibrators on the sky.

2.1 Extragalactic observations

The first set of observations planned was imaging of a region measuring $0\overset{\circ}{.}5 \times 2^\circ$, with one end centred on NGC 2559, a nearby galaxy, and the other end extending into the Galactic plane cirrus. NGC 2559 is a spiral galaxy at a distance of 20.8 Mpc (from the systemic velocity and assuming a Hubble constant of 75 km s^{-1}), with morphological type SB(s)bc pec (de Vaucouleurs et al. 1991). It was chosen as a target in this study since it is the IR-brightest nearby galaxy that lies in the SASSy area, and had not been previously observed by SCUBA. This section of sky was broken up into four $0\overset{\circ}{.}5 \times 0\overset{\circ}{.}5$ tiles, of which only two were observed during the S2SRO period – these were the outer ends of the strip, and hence are not contiguous. We refer to this as the 'extragalactic' pilot survey,

---

[1] Alternatively known as the SCUBA-2 Ambitious Sky Survey.

since (although relatively close to the Galactic plane) the field was chosen to contain a bright *IRAS* galaxy which had not previously been observed at submm wavelengths.

The region containing NGC 2559 was observed on 2010 February 27 and March 14, for a total of 167 min of observing yielding an average integration time of 27 s pixel^{-1}. The average optical depths at 225 GHz for the two nights were $\tau_{225} = 0.097$ and 0.154, the average noise-equivalent flux densities were 160 and 260 mJy s$^{-1/2}$, and the telescope scan rates were 240 and 360 arcsec s^{-1}, respectively. Data were reduced using the Sub-Millimetre User Reduction Facility (SMURF) map-maker (Chapin et al. 2010; Jenness et al. 2010; Chapin et al., in preparation), which we describe in more detail in the next section. The resulting raw map has a noise of 38 mJy beam^{-1} determined using the produced noise map.

The region about 1° away, containing known Galactic cirrus, was observed for a total of 105 min, resulting in an average integration time of 16 s pixel^{-1}. Both 'pong' and 'rotating pong' scan strategies (Kackley et al. 2010)[2] were used for the NGC 2559 field and only the rotating pong strategy for the cirrus field. Although NGC 2559 is readily detected in the resulting map of this area, we are unable to identify any Galactic cirrus within the other map. This is due to a combination of the relatively high noise level and the difficulty in detecting extended diffuse structure (largely removed in the reduction process). Therefore, for the remainder of this paper, of the two extragalactic observations, we restrict our attention to the map containing the galaxy NGC 2559.

2.2 Galactic observations

The second distinct set of observations targeted a field around the W5-E H II region. This region was selected because of its simple geometry and, at 2 kpc (e.g. Karr & Martin 2003), is one of the nearest regions of triggered massive star formation (Megeath et al. 2008). A single region of 1° × 1° was mapped on 2009 December 5, at a speed of 600 arcsec s^{-1} (the nominal scan rate for SASSy) using the 'pong' scanning mode (Kackley et al. 2010). The scan pattern had each successive sweep separated by 120 arcsec, ensuring an overlap to improve mapping performance.

The on-source time was 70 min which resulted in a total of 12 passes over the entire region. In addition, the central $0\overset{\circ}{.}5 \times 0\overset{\circ}{.}5$ was mapped at the same speed for another 70 min, covering that region 42 times, for a total observing time of 140 min. The average integration times per pixel for the inner and outer regions were 18 and 3 s, respectively. The 225-GHz optical depth varied from 0.08 to 0.12 with a mean of 0.10 (corresponding to Grade 3 weather). This is substantially lower than the allotted opacity band for SASSy; however, the central 0.25 deg^2 region of the map has a sensitivity slightly exceeding the SASSy target level, and therefore represents a valid test of the detectability of sources. The central portion of the map has a noise of 25 mJy beam^{-1}; the value for the outer region is 60 mJy beam^{-1}, as reported by the noise map. Note that 450-μm data were also obtained and reduced, but were found to be of limited use, with only the single brightest source being detected.

3 DATA REDUCTION AND SOURCE DETECTION

The raw time series data were processed using SMURF (Chapin et al. 2010; Jenness et al. 2010) called from the ORAC-DR pipeline (Gibb & Jenness 2010). SMURF solves for the astronomical signal using an iterative technique, fitting and filtering out noise contributions from the atmosphere and the instrument. Details of the map-maker may be found in Chapin et al. (in preparation). Readings from the JCMT water vapour monitor (Dempsey & Friberg 2008) and the values found by Dempsey et al. (2010) were used to correct for atmospheric extinction. The ORAC-DR pipeline was used to mosaic the individual observations using inverse-variance weighting.

In the NGC 2559 raw map, it is clear that time-dependent noise shows up as large-scale structure, obscuring the detection of the galaxy. This comes from a combination of residual sky fluctuations, as well as oscillations inherent to the instrument when these data were taken. Fig. 1 shows the NGC 2559 field after smoothing with the beam [to improve the signal-to-noise ratio (S/N) for sources]. The resulting map is dominated by structure at roughly the scale of the SCUBA-2 array. However, since the core of the galaxy shows up as a compact source, we are able to use a point source filter to make an unambiguous detection. The 'matched-filter' method implemented within ORAC-DR subtracts the map smoothed with a larger Gaussian (30 arcsec in this case) from the map convolved with a Gaussian equal to the JCMT beamsize (14 arcsec at 850 μm), thus giving a 'Mexican hat' type spatial filter. The resulting map is able to enhance sources that are approximately point-like (since we expect extragalactic sources found by SASSy to be approximately point-like). We experimented with different choices for filter shape, and found that the default within ORAC-DR is close to the best we can do in terms of S/N. In principle, we could improve things by using specific knowledge of the expected shape of NGC 2559, but that would not be helpful in a blind SASSy search (which is what we are preparing here).

Fig. 2 shows the NGC 2559 field after applying the matched-filter algorithm to remove the large-scale structure. NGC 2559 is now plainly visible in the centre of the map. Fig. 3 shows a histogram of the pixel values found in the matched-filtered map of NGC 2559.

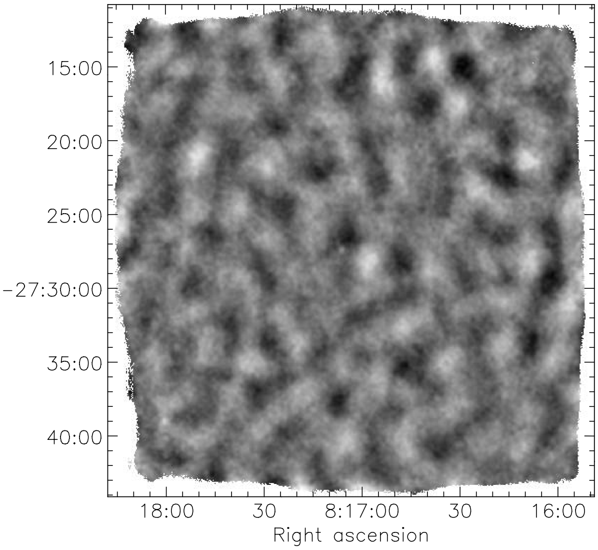

Figure 1. Smoothed S/N map of the 'extragalactic' field, being about $0\overset{\circ}{.}5$ across. NGC 2559 is located at the centre of this map, which is dominated by artefacts of roughly the SCUBA-2 array size.

---

[2] 'Pong' is the default scanning mode for covering large areas with SCUBA-2, and is like a raster-scanning pattern except that it is designed to visit different parts of the map on different time-scales. 'Rotating pong' means that the orientation of the pattern is allowed to rotate in sky coordinates as the observations are carried out, resulting in scans at many different angles, which is better from a map-making perspective.

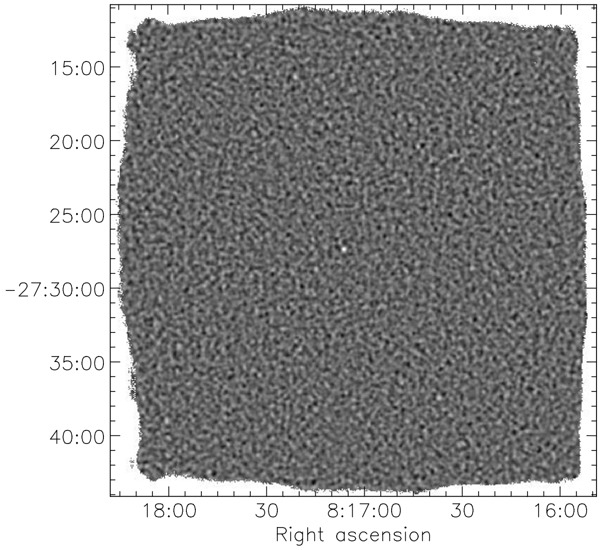

Figure 2. Matched-filtered S/N map of the 'extragalactic' field. NGC 2559 is located at the centre of this map, and is clearly detected. Other peaks in this map (near the north-east and south-east corners) appear to be just noise excursions.

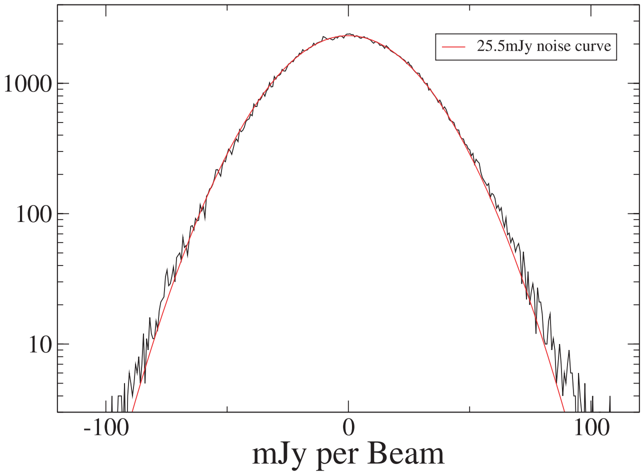

Figure 3. Histogram of matched-filtered pixel values in the 'extragalactic' map. This can be used to determine the spatial noise in the map. A 25.5 mJy noise curve is plotted for comparison, while the expected uncorrelated noise in the map is significantly smaller.

After removing the background variations in the map, the spatial noise is found to be approximately 25.5 mJy (equivalent for a point source). This is larger than the average noise of 19 mJy calculated by the data-reduction pipeline (i.e. given by the noise map), due to not having filtered out all the spatially correlated noise. Since shallow extragalactic fields should be composed of white noise plus a few sources, the S/N matched-filtered map is re-normalized to have an rms of unity before searching for sources. In other words, we are effectively using the spatial rms noise, rather than the purely white noise estimate which comes from the pipeline noise map.

Fig. 4 shows the W5-E Galactic star-forming region map, while Fig. 5 shows the related S/N map and Fig. 6 shows an annotated version with several previously catalogued regions labelled. Since the purpose of SASSy is to find and catalogue new sources for future study, it is simplest to ignore source structure and to filter the map with the matched filter. For objects within the Galactic strip, we use a 60-arcsec background subtraction for the matched filter. This scale is chosen since we expect Galactic sources to be more extended than extragalactic sources. Fig. 7 shows the W5-E map after being matched-filtered. The central $\sim 0\overset{\circ}{.}5 \times 0\overset{\circ}{.}5$ region has a spatial noise level of 15 mJy, while the outer region has a noise level of approximately 30 mJy, once processed by the matched filter (see Fig. 6). Note that these values are different from the noise values in the unfiltered map since they only apply to the detection of compact sources (and so should not be considered as being a noise 'per beam', as would be usual for extended structure).

Since the matched filters do affect the fluxes of extended sources, we have simulated extended Gaussian sources to determine the extent of this effect. Since the filter is optimized for point sources, their fluxes are unchanged. For the extragalactic matched filter (30 arcsec smoothed background subtraction), sources that appear to have an FWHM of 30 and 40 arcsec will result in a drop in peak flux by approximately 20 and 50 per cent, respectively, after applying the matched filter. For the galactic matched filter (60 arcsec smoothed background subtraction), sources that appears to have an FWHM of 60 and 80 arcsec will result in a drop in peak flux by approximately 20 and 50 per cent, respectively, after applying the matched filter. Despite filtering out extended emission, we find that we detect many more candidate sources after applying a matched filter than simply using the unfiltered map (27 compared with only eight). In principle, part of this increase could be due to a single extended source breaking up into multiple peaks after filtering. However, inspection of the results shows that this only happened for one source in the W5-E field. Thus, for the purposes of SASSy, the matched filter offers the best method of detecting faint compact sources for follow-up observations.

4 DETECTIONS

4.1 NGC 2559 field

In order to extract sources from the matched-filtered maps in a manner which could be easily automated for the full survey, we use the FELLWALKER algorithm (Berry et al. 2007), implemented in the Starlink software package CUPID. We use this algorithm simply to associate contiguous blocks of pixels with a single source – the brightness is estimated from the peak value in the match-filtered S/N map. Given the simple nature of the source detection, the choice of algorithm is not critical. A minimum number of pixels of seven and a low rms level are used in FELLWALKER to recover as many real and noise peaks as possible for producing histograms.

Fig. 8 shows a histogram of S/N peaks of all the sources within the NGC 2559 field. NGC 2559 is clearly detected at a S/N of about 7, and there are two other candidate sources at a S/N around 4.5. There are no obvious counterparts for these two sources in any relevant survey. The histogram shows that the detection of NGC 2559 is an outlier in the distribution, but the two other candidates seem consistent with the noise distribution, and in a map with $>10^4$ beamsize pixels they are not very unlikely. Nevertheless, we checked for counterparts in the 20-cm NVSS survey (Condon et al. 1998). We additionally extracted archival 20-cm Very Large Array (VLA) data of approximately the same depth (lower bandwidth but larger integration time), re-reduced them and added them to the NVSS data. No radio sources are detected in the combined 20-cm image at the positions of the two peaks in the SASSy map, where the noise level is 320–350 μJy.

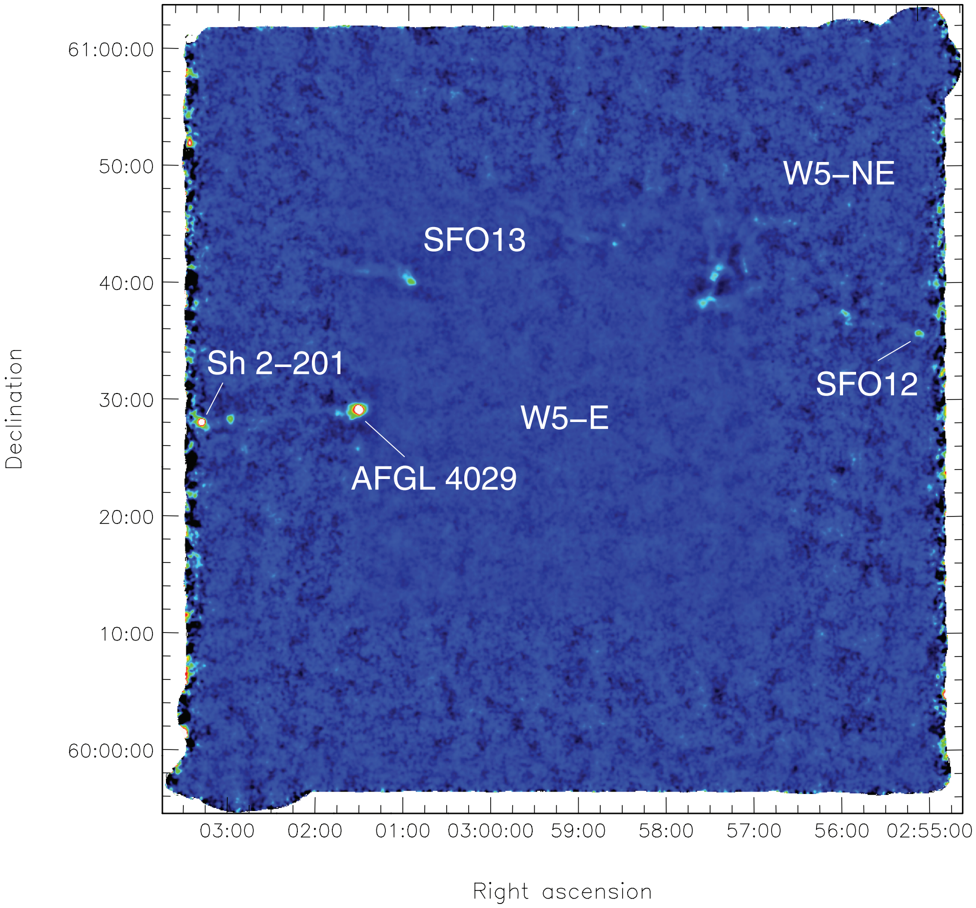

Figure 4. The W5-E star-forming region as mapped by SCUBA-2 at 850 μm, smoothed with a Gaussian with a full width at half-maximum (FWHM) of 14 arcsec. Colour scale ranges from −100 to +500 mJy beam^{-1}. The central roughly 1/4 of the map can be seen to have lower noise than the rest. Known objects are labelled, as is the approximate centre of the W5-E H II region.

We also explored different choices for the filtering, and found that although the detection of NGC 2559 is robust the next most significant peaks vary in position and brightness. The SASSy survey plan is to carry out short follow-up observations of such candidates to distinguish between real objects and false positives (whether just noise excursions or mapping artefacts). This pilot survey suggests that the level at which follow-up will be worthwhile is around the 5σ level for large maps.

Fig. 9 shows an optical image [from the Digitized Sky Survey (DSS)] of NGC 2559 with matched-filtered SCUBA-2 contours overlaid. NGC 2559 shows up at a flux density of 156 ± 26 mJy and would be detectable in data representative of SASSy (with target rms of 30 mJy).

4.2 W5-E field

Turning to the Galactic pilot map, this field contains a number of known sources, including three bright-rimmed clouds (SFO 12, 13 and 14), and the H II region Sh 2-201. Note that SFO 14 contains the massive young stellar object AFGL 4029. The three bright-rimmed clouds have all been detected previously at submm wavelengths using SCUBA (Morgan et al. 2008).

All of these sources are detected in the SCUBA-2 map with good to high significance. A total of 27 sources were identified at >6σ after applying the matched filter, most of which are unknown at submm wavelengths. The central portion of the map containing the W5-E H II region is devoid of dust emission. Table 1 lists the objects found with a S/N greater than 6 using the matched-filter method. Of the objects in Table 1, 11 are brighter than 150 mJy and would be detected by a blind SASSy survey at more than 5σ. Fig. 10 shows a histogram of S/N peaks of all the sources extracted from the W5-E map.

By inspecting the unfiltered map, it is clear that some of the ‘sources’ found in this way are parts of extended filamentary structures. Fig. 4 shows a number of extended, filamentary features of low S/N. While faint, they are undoubtedly real as they show good agreement with the CO data presented by Karr & Martin (2003) and Niwa et al. (2009), as well as *Spitzer* MIPS images (Koenig et al. 2008). However, in practice, mapping such low surface-brightness features is beyond the scope of SASSy and falls into the realm of follow-up observations triggered by detecting new compact sources. The most interesting Galactic sources found by SASSy will be relatively isolated, and they will be discovered through applying a simple automated source-extraction procedure similar to that used here. None the less, it is encouraging to find that SASSy is capable of detecting extended features and there are many approaches which can be taken to characterize such morphology. Further experience with SASSy data will guide our approach.

Of all the new submm detections, perhaps the most striking source in the SCUBA-2 map is that labelled as the ‘cold core’ in Fig. 5. It shows up clearly in the S/N map at a significance of 7σ. Comparison with *Spitzer* data reveals that while it is also detected at 160 and

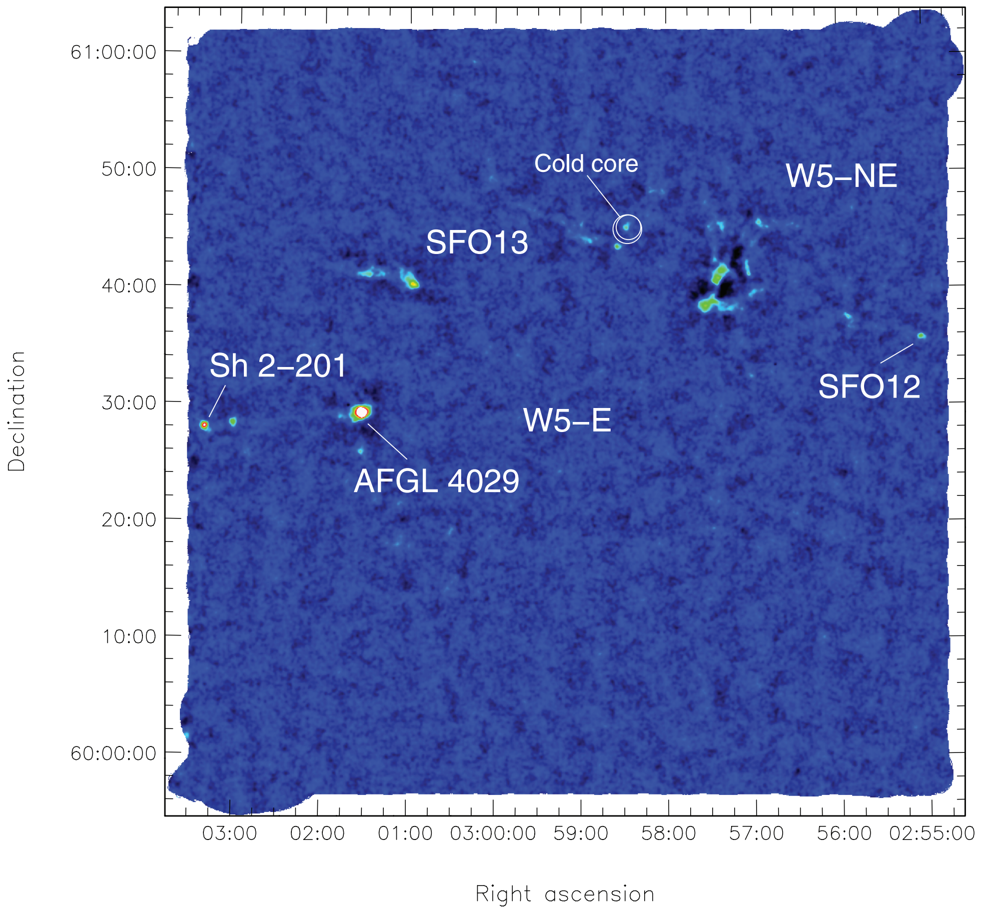

Figure 5. S/N image for W5-E. The colour scale ranges from −2 to +10. The ‘cold core’ referred to in the text is circled. Known objects are labelled, as is the approximate centre of the W5-E H II region.

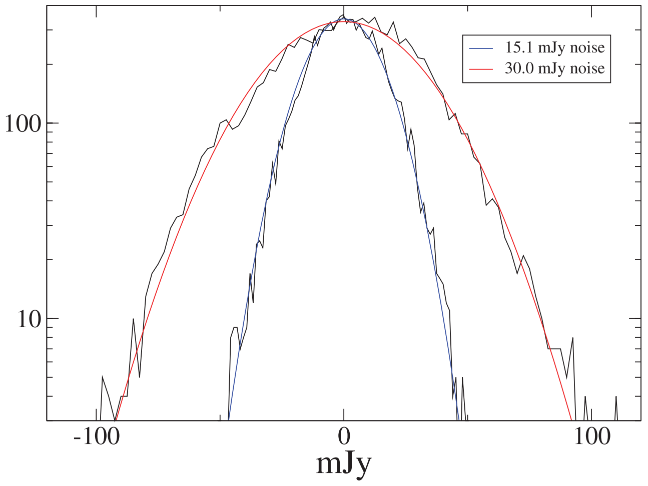

Figure 6. Histogram of matched-filtered pixel values in the W5-E map for 100 pixel^2 blank sections of the inner and outer regions of the map. Noise curves were fitted and determined to be 15 and 30 mJy, respectively.

70 µm, it is completely absent at 24 µm. As shown in Fig. 11, the SCUBA-2 source lies within the boundary of a bright-rimmed cloud, externally illuminated by the O stars in the W5-E cluster. This source appears to be cold, a conclusion which is confirmed by our analysis below.

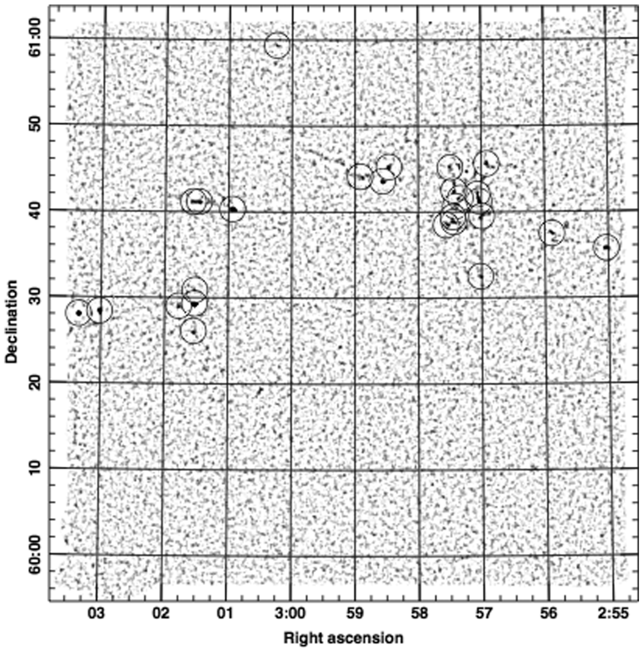

Figure 7. The matched-filtered map of W5-E with circles indicating the $>6\sigma$ sources listed in Table 1.

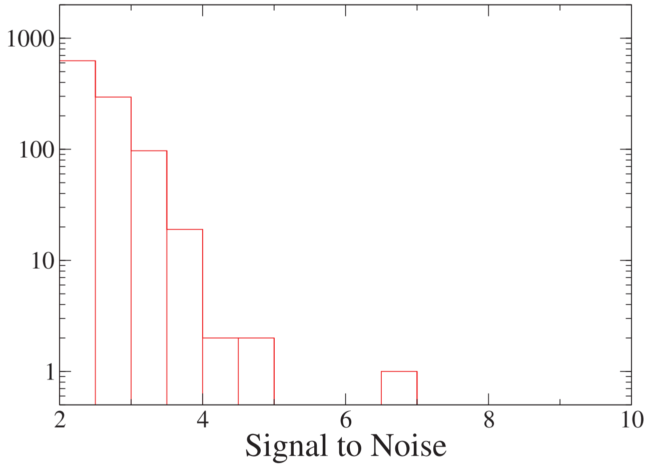

Figure 8. Histogram of peak S/N values within the matched-filtered NGC 2559 field. NGC 2559 itself shows up at around 6.6σ, while the two candidate sources at about 4.5σ appear to be noise bumps (note that a 4σ event is not very unlikely, given the number of pixels in this map).

Table 1. List of objects found with a peak S/N greater than 6 in the W5-E region using the matched-filter method.

S_{850} (mJy)	(S/N)	Position (J2000) RA ($^{\mathrm{h\,m\,s}}$)	Dec. ($^{\circ\,\prime\,\prime\prime}$)
2290	163	03:01:31.783	+60:29:19.81
1970	44.2	03:03:21.039	+60:28:03.98
410	16.0	02:55:01.806	+60:35:43.70
405	18.0	03:03:01.319	+60:28:24.23
236	18.1	03:00:56.349	+60:40:20.11
226	9.0	02:56:54.974	+60:45:37.30
212	8.6	02:55:53.335	+60:37:29.14
185	15.2	02:58:33.795	+60:43:36.67
172	12.6	02:57:02.215	+60:41:15.56
164	6.7	03:01:46.608	+60:29:03.05
152	13.8	02:57:24.688	+60:40:40.34
131	11.6	02:57:33.643	+60:38:28.77
130	6.7	03:00:14.481	+60:59:22.56
119	9.1	03:01:32.609	+60:26:08.48
118	10.5	02:58:27.730	+60:45:15.82
112	9.6	02:57:26.183	+60:38:51.92
110	8.4	02:57:03.894	+60:42:04.86
108	10.1	02:57:19.897	+60:41:37.63
99	8.2	02:57:26.221	+60:42:31.99
89	6.2	03:01:31.556	+60:30:53.96
87	7.7	02:57:27.009	+60:39:26.70
79	6.0	02:58:55.106	+60:44:08.31
77	7.7	03:01:27.812	+60:41:10.03
75	6.6	02:57:01.063	+60:32:31.05
71	6.1	02:56:59.793	+60:39:31.14
69	6.2	02:57:29.653	+60:45:10.17
68	6.2	03:01:33.497	+60:41:10.29

5 PROPERTIES OF NGC 2559

5.1 Ancillary data

We complement the SASSy observations of NGC 2559 with available archival mid- and far-IR (FIR) data. NGC 2559 has been observed by both *IRAS* and *AKARI*, providing spectral coverage from 9 to 160 μm. These data can be used to constrain the spectral energy distribution (SED) of the source.

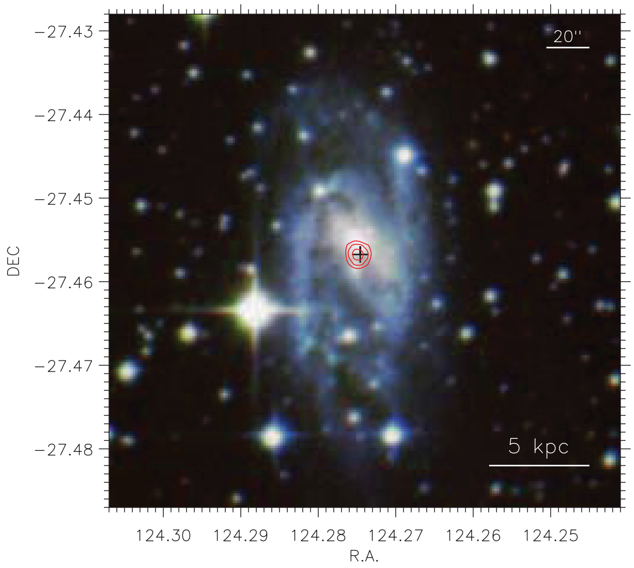

Figure 9. SCUBA-2 850 μm 5σ and 7σ contours overlaid on an optical three-colour image of NGC 2559 (derived from DSS data). The black cross marks the position of the NVSS radio source.

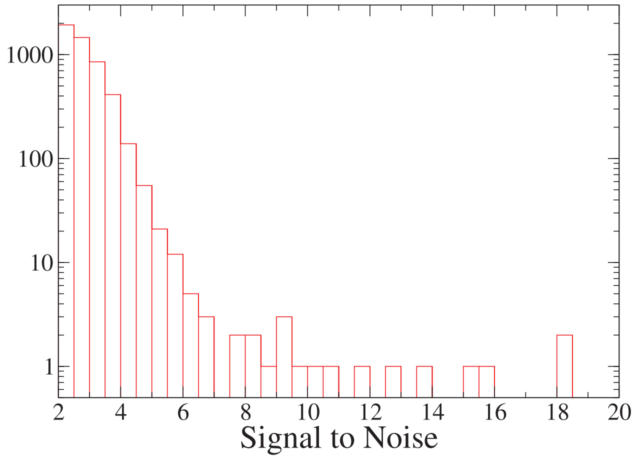

Figure 10. Histogram of peak S/N values within the matched-filtered W5-E field. The brightest W5-E source (AFGL 4029) has a S/N of over 100 and is not shown.

We estimate *IRAS* fluxes using the *IRAS* Scan Processing and Integration Tool (SCANPI[3]). Standard reduction parameters were used, taking into account the observed size of the galaxy (~3 arcmin; Prugniel & Heraudeau 1998; Jarrett et al. 2003) as an additional constraint. Although NGC 2559 is actually detected as a point source in all *IRAS* bands, we assume a minimum distance of 6 arcmin from the nominal position of the source for background subtraction. We obtain *AKARI* fluxes at 9 and 18 μm from the *AKARI*/IRC All-Sky Survey Point Source Catalogue (Ishihara et al. 2010), and at 65, 90 and 140 μm from the *AKARI*/FIS All-Sky Survey Bright Source Catalogue (Yamamura et al. 2010). We decide not to use the 160 μm

---

[3] Available at http://scanpiops.ipac.caltech.edu/9000/applications/Scanpi/index.html

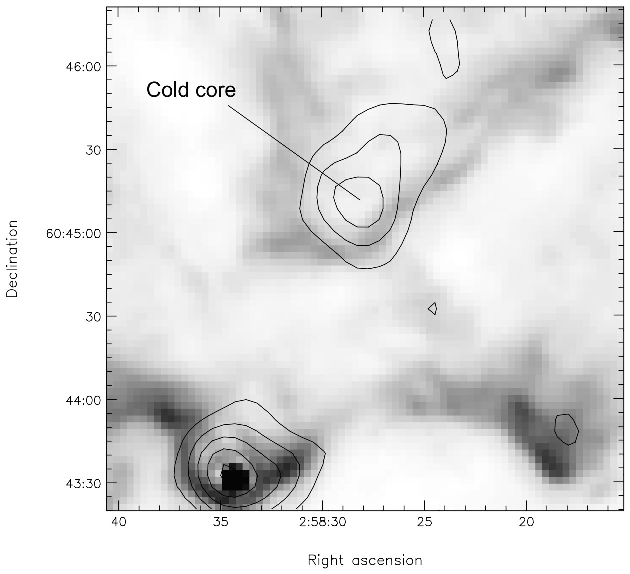

Figure 11. SCUBA-2 contours overlaid on *Spitzer* 24-μm image. The source labelled 'cold core' is circled and shows up clearly in the submm, yet within a dark region of the *Spitzer* image. It is, however, detected at 70 and 160 μm with *Spitzer*.

Table 2. The observed SED of NGC 2559. Flux densities and respective errors are in Jy. Quoted errors include an additional 20 per cent calibration uncertainty.

λ (μm)	S_ν	δS_ν	Instrument
9	1.5	0.3	*AKARI*/IRC
12	1.4	0.3	*IRAS*
18	1.8	0.4	*AKARI*/IRC
25	2.8	0.6	*IRAS*
60	26	5	*IRAS*
65	23	5	*AKARI*/FIS
90	39	8	*AKARI*/FIS
100	66	13	*IRAS*
140	52	12	*AKARI*/FIS
450	2.3	2.3	SCUBA-2 (u.l.)
850	0.156	0.04	SCUBA-2

measurement owing to the extremely high noise affecting this band: this is confirmed by the χ^2 increasing by about a factor of 2 when this measurement is included in our fits. In addition to that, we estimate an upper limit on the 450-μm flux from the shorter wavelength SCUBA-2 map. A 20 per cent uncorrelated uncertainty is applied to all data. The observed mid-IR to FIR data of NGC 2559 are given in Table 2.

5.2 SED fitting: dust models

We fit the dust models of Draine & Li (2007)[4] to the compilation of available data. These models provide the dust emissivity per hydrogen atom, $j_\nu(q_{\rm PAH}, U_{\rm min}, U_{\rm max})$, which is a function of three parameters: the fraction of dust mass in polycyclic aromatic hydrocarbons (PAHs), $q_{\rm PAH}$; the intensity of the radiation field from stars heating the interstellar medium (ISM), $U_{\rm min}$, and the intensity of the radiation field in photodissociation regions (PDRs), $U_{\rm max}$.

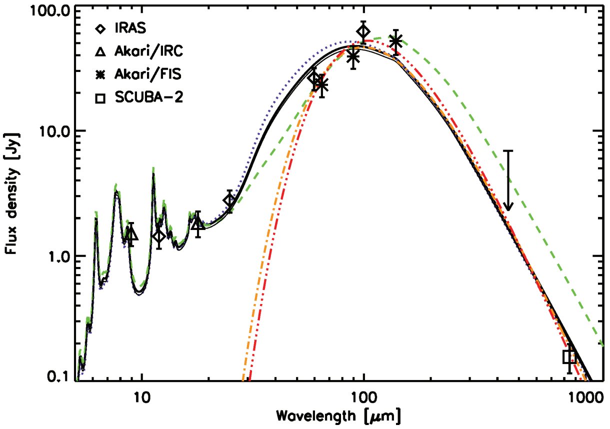

Figure 12. The observed FIR and submm SED of NGC 2559, together with dust model fits. An arrow marks the 3σ upper limit at 450 μm. The solid (black) line shows the best fit to all available data points. The dotted (blue) line is the best fit to the data set excluding the *AKARI*/FIS data. The thin solid (black) line is the best fit to the data set excluding the *IRAS* data. The dashed (green) line is the best-fitting model without the SCUBA-2 points. The dot–dashed (orange) line is the modified blackbody fit with $\beta = 2$. The triple-dot–dashed (red) line is the modified blackbody fit with free β. Error bars include an uncorrelated 20 per cent uncertainty.

We apply the same general method explained in Draine & Li (2007), but we use only the seven Milky Way dust model sets, as in Wiebe et al. (2009). Accordingly, we also set $U_{\rm max} = 10^6$ (we tested the reliability of this assumption by leaving $U_{\rm max}$ as a free parameter and found that the fit returns the same value). We thus fit to the observed SED a linear combination of diffuse ISM models (with $U_{\rm max} = U_{\rm min}$) and PDR models:

$$F_\nu(q_{\rm PAH}, U_{\rm min}, U_{\rm max}) \propto \frac{M_{\rm d}}{m_{\rm H} D^2} \times [(1-\gamma) j_\nu(q_{\rm PAH}, U_{\rm min}, U_{\rm min}) + \gamma j_\nu(q_{\rm PAH}, U_{\rm min}, U_{\rm max})]\,,$$

where $M_{\rm d}$ is the dust mass, $m_{\rm H}$ is the mass of a hydrogen atom and $D = 20.8$ Mpc is the distance to the galaxy. We then use the derived values to evaluate the dust-weighted starlight intensity $\langle U \rangle$. The best-fitting values for the parameters are found through χ^2 minimization. Fig. 12 shows the observed SED and best-fitting curves.

We note that the *AKARI*/FIS data are systematically low with respect to the *IRAS* data. We thus evaluate the outcome of the fit using either the full data set or a subset to assess the effect of this offset. Table 3 summarizes the different fits and results.

Fitting the dust models to the full set of data points available yields a reasonable fit, although the χ^2 is relatively high. We obtain the values $q_{\rm PAH} = 3.2$, $\gamma = 0.01$, $U_{\rm min} = 20$ and $\langle U \rangle = 21.9$. We derive a dust mass of $1.5 \times 10^7\,{\rm M}_\odot$ and a FIR luminosity of $2.0 \times 10^{10}\,{\rm L}_\odot$, from which we calculate a star formation rate (SFR) of $2.8\,{\rm M}_\odot\,{\rm yr}^{-1}$ using the relation of Bell (2003). The derived dust mass is about two times larger than the value obtained by Bettoni, Galletta & García-Burillo (2003), who find a value of $8.3 \times 10^6\,{\rm M}_\odot$ from data at 60 and 100 μm.

Note that the SFR can also be estimated using the 20-cm radio flux density along with the FIR/radio correlation (e.g. Condon 1992; Cram et al. 1998; Hopkins et al. 2001). With $S_{1.4} = 260$ mJy, this gives an SFR of around $10\,{\rm M}_\odot\,{\rm yr}^{-1}$, which is fairly consistent with the results obtained from the FIR fit.

---

[4] Available at http://www.astro.princeton.edu/~draine/dust/dust.html

Table 3. Draine & Li (2007) model parameters for NGC 2559 and derived physical quantities.

Data removed	χ^2	Degrees of freedom	q_{PAH}	U_{min}	$\langle U\rangle$	γ	M_{d} ($10^7\,\mathrm{M}_{\odot}$)	L_{FIR} ($10^{10}\,\mathrm{L}_{\odot}$)	SFR ($\mathrm{M}_{\odot}\,\mathrm{yr}^{-1}$)
None	17.7	7	3.2	20	21.9	0.01	1.5	2.0	2.8
AKARI/FIS	10.8	4	3.2	25	27.4	0.01	1.3	2.1	3.0
IRAS	10.7	3	4.6	20	22.0	0.01	1.5	1.9	2.7
SCUBA-2	3.5	5	4.6	5	5.6	0.01	5.7	2.2	3.1

Exclusion of the *AKARI*/FIS data points yields again a fit which correctly matches the SCUBA-2 850-μm point. Best-fitting parameters are rather similar, the only noticeable change being the increase of $U_{\mathrm{min}} = 25$ and of $\langle U\rangle = 27.4$, with the resulting dust mass, FIR luminosity and SFR fairly consistent with the previous fit.

Removing the *IRAS* points from the data set yields a similar fit with a χ^2 of 10.7 with three degrees of freedom. The fit parameters are almost undistinguishable from the first fit at $\lambda \geq 30$ μm.

For comparison, we also fit the models after excluding the SCUBA-2 point and upper limit. We obtain lower values of $U_{\mathrm{min}} = 5$ and $\langle U\rangle = 5.6$. But now the best fit misses the 850-μm flux density by about a factor of 4.

This shows the strong leverage of the SCUBA-2 data to properly constrain the FIR and submm SEDs of galaxies. In particular, in addition to the dust mass, the value of the starlight intensity U_{min} (and consequently $\langle U\rangle$) is strongly sensitive to the 850-μm flux density.

5.3 SED fitting: modified blackbody

For comparison with the more detailed Draine & Li (2007) models, we also fit a modified blackbody spectrum to the observed data. The fit is carried out assuming a shape for the modified blackbody described by the expression

$$S_\nu = \frac{M_{\mathrm{d}}\kappa}{D^2}\left(\frac{\nu}{\nu_0}\right)^{\beta} B_\nu(T), \qquad (1)$$

where $\nu_0 = 1.2\,\mathrm{THz} = c/(250\,\mu\mathrm{m})$, κ is the dust mass absorption coefficient at ν_0, β is the dust emissivity index and M_{d} is the dust mass. Once again, the best-fitting parameters are found by χ^2 minimization. We assume a mean value of $\kappa = 0.29\,\mathrm{m}^2\,\mathrm{Kg}^{-1}$ (see e.g. Wiebe et al. 2009, although there is considerably uncertainty in this value) and fix $\beta = 2$.

This modified blackbody fit yields consistent values of M_{d}, L_{FIR} and SFR with respect to the detailed dust models. Table 4 summarizes the modified blackbody results, and the fitted curves are shown in Fig. 12. We see that the dust temperature of NGC 2559 is around 26–29 K. This is warmer than for most of the galaxies studied in the SINGS sample (Draine et al. 2007), as well as those studied using BLAST (Wiebe et al. 2009). This is consistent with requiring a relatively higher value of U than for those other galaxies.

6 SOURCE PROPERTIES IN W5-E

From our catalogue of compact sources within the W5-E region we select two example sources, representative of two extreme regimes: (i) the brightest source in the field, AFGL 4029 (Deharveng et al. 1997 and references therein), and (ii) a fainter source to the north-west of the first, as an example of a potentially colder core (labelled 'cold core' in Fig. 5). The SCUBA-2 flux densities for both sources were obtained from photometry within an aperture of 30-arcsec diameter.

Ancillary data available for this region include *Spitzer* MIPS 70-μm observations of the whole field, as well as *IRAS*, *AKARI* coverage and SCUBA imaging for part of the field. The SCUBA-2 data are in excellent agreement with the SCUBA measurements, being consistent within errors, but covering a much wider area. We show *Spitzer* 70-μm contours on top of the SCUBA-2 image in Fig. 13.

The bright source AFGL 4029 is detected in almost all wavebands, having upper limits only at 65 and 90 μm. We fit a modified blackbody spectrum to the observed SED, after adding a 20 per cent uncorrelated uncertainty to the errors, as we did for NGC 2559. Leaving β as a free parameter in the fit yields a value of $\beta = 2.02$, which suggests that $\beta = 2$ is a good assumption for the dust emissivity index. We derive a temperature $T = 31$ K and a dust mass of $60\,\mathrm{M}_{\odot}$, with a FIR luminosity of $5000\,\mathrm{L}_{\odot}$. This is in reasonable agreement with the value of $3200\,\mathrm{L}_{\odot}$ estimated by Morgan et al. (2008).

The faint source is detected only at 70 and 850 μm. A relatively nearby 90-μm source is detected by *AKARI*; however, its position is offset by 28 arcsec from the *Spitzer* position. Although this lies within the point spread function of *AKARI* at 90 μm, we prefer not to use this measurement in our analysis to avoid contamination by other potential sources (and in any case it adds little to the 70-μm constraint). Reliable flux densities were obtained from the *Spitzer* 24 and 70 μm images, using the same 30-arcsec aperture as for the SCUBA-2 data. While the cold core is also evident in the 160-μm MIPS image, the presence of significant artefacts prevents the extraction of a useful flux measurement.

Although only two photometry points are available, a fit to the SED using again a modified blackbody with $\beta = 2$ yields reasonable quantities and confirms this source to be a cold protostellar core. We obtain a temperature $T = 17$ K, FIR luminosity of $27\,\mathrm{L}_{\odot}$ and a dust mass of $11\,\mathrm{M}_{\odot}$. Comparing the *AKARI* 90-μm point to the fit shows that the measurement is in excellent agreement with the

Table 4. Modified blackbody fits for NGC 2559 and derived physical quantities.

Fit	χ^2	Degrees of freedom	β	T_{d} (K)	M_{d} ($10^7\,\mathrm{M}_{\odot}$)	L_{FIR} ($10^{10}\,\mathrm{L}_{\odot}$)	SFR ($\mathrm{M}_{\odot}\,\mathrm{yr}^{-1}$)
Fixed β	6.0	5	2	29	0.31	1.8	2.6
Free β	4.7	4	2.3	26	0.47	2.0	2.8

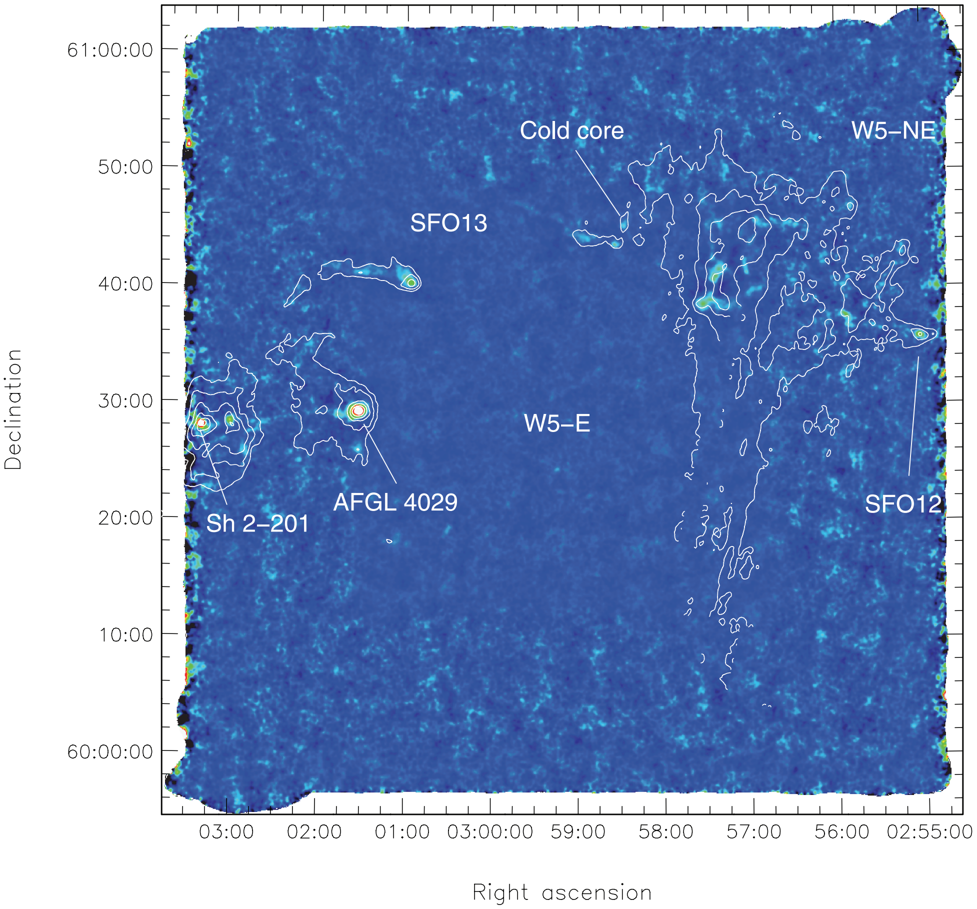

Figure 13. SCUBA-2 850-μm emission in colour with *Spitzer* 70-μm contours overlaid. Sources are labelled as in Fig. 4. The *Spitzer* contours do not close to the south of W5-NE due to a lack of coverage there.

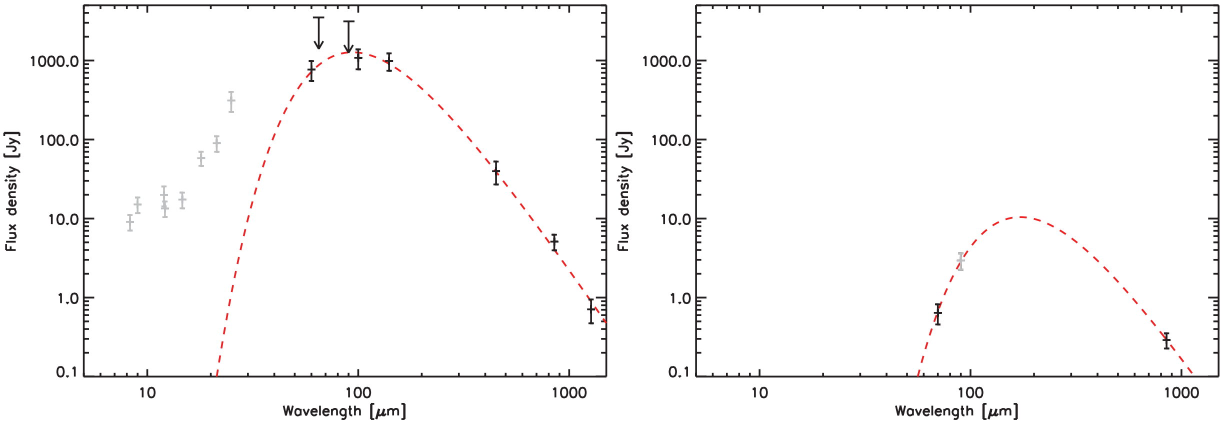

Figure 14. The observed FIR and submm SED of AFGL 4029 and of the cold source in W5-E. Black points are used for the fit, arrows mark upper limits. The dotted (red) line is the modified blackbody fit with $\beta = 2$.

expected flux density, suggesting that this might actually be the counterpart to the same source. The result of the fit for both sources is shown in Fig. 14.

The readiness with which we were able to pick out a relatively cold source, even in this small pilot study, shows that SASSy will be able to detect single low-mass cold clumps inside larger star-forming regions. Detailed follow-up of such sources will determine where they lie on the star formation sequence.

7 DISCUSSION

With the current SASSy S2SRO observations, we have shown that we will be able to detect and catalogue real sources, both Galactic and extragalactic. Based on early commissioning estimates, SCUBA-2 mapping during S2SRO was expected to be approximately 50 times faster than for SCUBA. A direct comparison with the SCUBA data in the W5-E field shows the mapping speed improvement factor to be 60, after scaling the map sizes and noise levels. Assuming similar weather conditions and a similar efficiency for the new science-grade arrays currently being commissioned on SCUBA-2, SASSy should be able to map the sky at a rate of $>0.8\,\mathrm{deg}^2\,\mathrm{h}^{-1}$ to the target sensitivity, exceeding the capabilities of SCUBA by hundreds of times. However, the performance of the new 850-μm arrays are currently unknown, since they are yet to be tested on the sky, and hence the area which will be ultimately mappable by SASSy is still uncertain. At the present time SCUBA-2 has all eight arrays installed and is undergoing the first stages of full commissioning. It is anticipated that this will be completed in mid-2011 and the instrument made available to the community as soon as possible thereafter. SASSy will therefore start in earnest some time in 2011.

Nevertheless, these initial data have shown that it is possible to reach a 1σ sensitivity to point sources of $\sim$30 mJy while scanning rapidly with SCUBA-2 in relatively mediocre weather conditions. The map-making and source extraction procedures are fast and require little in the way of human intervention. Experience with this pilot programme has already been fed back directly into the software pipeline and most of the data processing and analysis is now automated.

The science case for SASSy remains strong and has been made stronger by recent *Herschel* discoveries. There is still a pressing need for a wide-area shallow 850-μm survey in the era of *Herschel*, *Planck* and ALMA. This pilot study has shown that it is feasible to find sources in the shallow maps which SCUBA-2 will soon produce routinely.

ACKNOWLEDGMENTS

The James Clerk Maxwell Telescope is operated by The Joint Astronomy Centre on behalf of the Science and Technology Facilities Council of the United Kingdom, the Netherlands Organisation for Scientific Research and the National Research Council of Canada. Data for this paper were taken as part of the S2SRO programme, with Project ID M09BI142. This research used the facilities of the Canadian Astronomy Data Centre operated by the National Research Council of Canada with the support of the Canadian Space Agency. This research was supported by the Canadian Natural Sciences and Engineering Research Council and enabled through funding from the Canada Foundation for Innovation and through the CANFAR Programme, funded by CANARIE, Canada's advanced Internet organization. This work is based in part on observations made with the *Spitzer Space Telescope*, which is operated by the Jet Propulsion Laboratory, California Institute of Technology, under a contract with NASA. This research is based in part on observations with *AKARI*, a JAXA project with the participation of ESA. This research has made use of the NASA/IPAC Extragalactic Database (NED) which is operated by the Jet Propulsion Laboratory, California Institute of Technology, under contract with NASA. The Digitized Sky Surveys were produced at the Space Telescope Science Institute under US Government grant NAG W-2166. The images of these surveys are based on photographic data obtained using the Oschin Schmidt Telescope on Palomar Mountain and the UK Schmidt Telescope. The VLA is part of the US National Radio Astronomy Observatory, a facility of the National Science Foundation operated under cooperative agreement by Associated Universities, Inc.

REFERENCES

Bell E., 2003, ApJ, 586, 794

Berry D., Reinhold K., Jenness T., Economou F., 2007, in Shaw R. A., Hill F., Bell D. J., eds, ASP Conf. Ser. Vol. 376, Astronomical Data Analysis Software and Systems XVI. Astron. Soc. Pac., San Francisco, p. 425

Bettoni D., Galletta G., García-Burillo S., 2003, A&A, 405, 5

Chapin E., Gibb A., Jenness T., Berry D., Scott D., 2010, The Sub-Millimetre User Reduction Facility, Starlink User Note 258, Version 1.0.0 (http://www.starlink.ac.uk/docs/sun258.htx/sun258.html)

Condon J., 1992, ARA&A, 30, 575

Condon J., Cotton W., Greisen E., Yin Q., Perley R., Taylor G., Broderick J., 1998, ApJ, 115, 1693

Cram L., Hopkins A., Mobasher B., Rowan-Robinson M., 1998, ApJ, 507, 155

de Vaucouleurs G., de Vaucouleurs A., Corwin H., Jr, Buta R., Paturel G., Fouque P., 1991, Third Reference Catalogue of Bright Galaxies. Springer-Verlag, Berlin

Deharveng L., Zavagno A., Cruz-Gonzalez I., Salas L., Caplan J., Carrasco L., 1997, A&A, 317, 459

Dempsey J., Friberg P., 2008, in Stepp L. M., Gilmozzi R., eds, Proc. SPIE Vol. 7012, Ground-based and Airborne Telescopes II. SPIE, Bellingham, p. 70123Z

Dempsey J. T., Friberg P., Jenness T., Bintley D., Holland W. S., 2010, in Holland W. S., Zmuidzinas J., eds, Proc. SPIE Vol. 7741, Millimeter, Submillimeter, and Far-Infrared Detectors and Instrumentaion for Astronomy V. SPIE, Bellingham, p. 77411X

Draine B., Li A., 2007, ApJ, 657, 810

Draine B. et al., 2007, ApJ, 663, 866

Gibb A., Jenness T., 2010, Processing SCUBA-2 Data with ORAC-DR, Starlink User Note 264, Version 1.0.0 (http://www.starlink.ac.uk/docs/sun264.htx/sun264.html)

Holland W. et al., 1999, MNRAS, 303, 659

Holland W., Duncan W., Kelly B., Irwin K., Walton A., Ade P., Robson E., 2003, in Phillips T. G., Zmuidzinas J., eds, Proc. SPIE Vol. 4855, Millimeter and Submillimeter Detectors for Astronomy. SPIE, Bellingham, p. 1

Holland W. et al., 2006, in Zmuidzinas J., Holland W. S., Withington S., Duncan W. D., eds, Proc. SPIE Vol., 6275, Millimeter and Submillimeter Detectors and Instrumentaion for Astronomy III. SPIE, Bellingham, 62751E

Hopkins A., Connolly A., Haarsma D., Cram L. E., 2001, AJ, 122, 288

Ishihara D. et al., 2010, A&A, 514, 1

Jarrett T., Chester T., Cutri R., Schneider S., Huchra J., 2003, AJ, 125, 525

Jenness T., Berry D., Chapin E., Economou F., Gibb A., Scott D., 2010 preprint (arXiv:1011.5876)

Kackley R., Scott D., Chapin E., Friberg P., 2010, in Radziwill N. M., ed., Proc. SPIE Vol. 7740, Software and Cyberinfrastructure for Astronomy. SPIE, Bellingham, 77401Z

Karr J., Martin P., 2003, ApJ, 595, 900

Koenig X., Allen L., Gutermuth R., Hora J., Brunt C., Muzerolle J., 2008, ApJ, 688, 1142

Megeath S., Townsley L., Oey M., Tieftrunk A. R., 2008, in Reipurth B., ed., Handbook of Star Forming Regions: Volume 1, The Northern Sky. Astron. Soc. Pac., San Francisco, p. 264

Morgan L., Thompson M., Urquhart J., White G., 2008, A&A, 477, 557

Negrello M. et al., 2010, Sci, 330, 800

Niwa T., Itoh Y., Oasa Y., Sunada K., Sugitani K., Mukai T., 2009, A&A, 500, 1119

Prugniel P., Heraudeau P., 1998, A&AS, 128, 299

Thompson M. A., Serjeant S., Jenness T., Scott D., Ashdown M., Brunt C., Butner H., 2007, preprint (arXiv:0704.3202v2)

Ward-Thompson D. et al., 2010, A&A, 518, L92

Wiebe D. et al., 2009, ApJ, 707, 1809

Yamamura I., Makiuti S., Ikeda N., Fukuda Y., Oyabu S., Koga T., White G., 2010, VizieR Online Data Catalog, 2298, 0

This paper has been typeset from a TEX/LATEX file prepared by the author.